The Layered Ternary Germanium Tellurides $ZrGeTe_4$, $HfGeTe_4$, and $TiGeTe_6$: Structure, Bonding, and Physical Properties

Arthur Mar and James A. Ibers*

Contribution from the Department of Chemistry, Northwestern University, Evanston, Illinois 60208-3113

Received October 22, 1992

Abstract: The new ternary chalcogenides zirconium germanium tetratelluride ($ZrGeTe_4$), hafnium germanium tetratelluride ($HfGeTe_4$), and titanium germanium hexatelluride ($TiGeTe_6$) have been synthesized, and their structures have been determined by single-crystal X-ray diffraction methods. The compounds $ZrGeTe_4$ and $HfGeTe_4$ are isostructural. They crystallize in space group C_{2v}^{12}-$Cmc2_1$ of the orthorhombic system with four formula units in cells of dimensions a = 3.976(4), b = 15.876(16), c = 10.948(12) Å ($ZrGeTe_4$) and a = 3.963(3), b = 15.875(10), c = 10.941(7) Å ($HfGeTe_4$) at 113 K. The compound $TiGeTe_6$ crystallizes in space group C_{2h}^3-$C2/m$ of the monoclinic system with four formula units in a cell of dimensions a = 13.972(26), b = 3.909(9), and c = 17.454(32) Å and β = 104.95(5)° at 113 K. These compounds adopt new layered structure types, in which the basic structural building blocks are metal-centered bicapped trigonal prisms, one of whose caps is a $GeTe_3$ trigonal pyramid. The structure of $MGeTe_4$ (M = Zr, Hf) consists of true two-dimensional layers $^2_\infty[MGeTe_4]$, while that of $TiGeTe_6$ consists of one-dimensional chains $^1_\infty[Ti_2Ge_2Te_{12}]$ that are weakly linked together by long Te–Te bonds to form a layer. Structural interrelationships among these compounds and some binary chalcogenides are presented. The compounds $ZrGeTe_4$ and $HfGeTe_4$ are semiconductors; they are probably nonstoichiometric. The compound $TiGeTe_6$ appears to undergo a metal-to-semiconductor transition below 165 K. Extended Hückel band-structure calculations are used to rationalize the physical properties and bonding features in these compounds.

Introduction

In recent years, an increasing number of ternary tellurides have been synthesized and characterized by this and other groups,[1-23] remedying somewhat the paucity of tellurides that had long existed when compared to the sulfides and selenides. Most of these studies have concentrated on ternary tellurides of the *group V* transition metals Nb and Ta, reflecting the rich structural chemistry[24,25] that these elements also possess in their binary chalcogenides. In contrast, far fewer ternary tellurides of the *group IV* transition metals Ti, Zr, and Hf are known, although we have expended much effort in exploring these systems. The unusual properties (e.g., charge-density waves,[25-33] superconductivity,[34-38] and intercalation chemistry[39,40]) that are imparted by the low-dimensional character of many of the binary chalcogenides provide a strong motivation for discovering new compounds in these systems.

In view of the common coordination preferences that are shared by the group IV and V elements in their binary chalcogenides (e.g., bicapped trigonal prisms in $ZrSe_3$ and $TaSe_3$),[41-43] we anticipated similarly related ternary compounds, but clearly

(1) Liimatta, E. W.; Ibers, J. A. *J. Solid State Chem.* **1987**, *71*, 384–389.
(2) Liimatta, E. W.; Ibers, J. A. *J. Solid State Chem.* **1988**, *77*, 141–147.
(3) Liimatta, E. W.; Ibers, J. A. *J. Solid State Chem.* **1989**, *78*, 7–16.
(4) Mar, A.; Ibers, J. A. *J. Chem. Soc., Dalton Trans.* **1991**, 639–641.
(5) Mar, A.; Ibers, J. A. *J. Solid State Chem.* **1991**, *92*, 352–361.
(6) Mar, A.; Ibers, J. A. *J. Solid State Chem.* **1992**, *97*, 366–376.
(7) Mar, A.; Jobic, S.; Ibers, J. A. *J. Am. Chem. Soc.* **1992**, *114*, 8963–8971.
(8) Keane, P. M.; Ibers, J. A. *Inorg. Chem.* **1991**, *30*, 1327–1329.
(9) Keane, P. M.; Ibers, J. A. *J. Solid State Chem.* **1991**, *93*, 291–297.
(10) Keane, P. M.; Ibers, J. A. *Inorg. Chem.* **1991**, *30*, 3096–3098.
(11) Mitchell, J. F.; Burdett, J. K.; Keane, P. M.; Ibers, J. A.; DeGroot, D. C.; Hogan, T. P.; Schindler, J. L.; Kannewurf, C. R. *J. Solid State Chem.* **1992**, *99*, 103–109.
(12) Keane, P. M.; Lu, Y.-J.; Ibers, J. A. *Acc. Chem. Res.* **1991**, *24*, 223–229.
(13) Huang, B.; Huang, J.; Liu, S. *Jiegou Huaxue* **1989**, *8*, 145–148.
(14) Huang, J.; Huang, B. *Jiegou Huaxue* **1988**, *7*, 214–217.
(15) Huang, B.; Shang, B.; Huang, J. *Jiegou Huaxue* **1988**, *7*, 133.
(16) Badding, M. E.; DiSalvo, F. J. *Inorg. Chem.* **1990**, *29*, 3952–3954.
(17) Li, J.; Hoffmann, R.; Badding, M. E.; DiSalvo, F. J. *Inorg. Chem.* **1990**, *29*, 3943–3952.
(18) Monconduit, L.; Evain, M.; Boucher, F.; Brec, R.; Rouxel, J. *Z. Anorg. Allg. Chem.* **1992**, *616*, 177–182.
(19) Li, J.; Carroll, P. J. *Mater. Res. Bull.* **1992**, *27*, 1073–1081.
(20) Tremel, W. *J. Chem. Soc., Chem. Commun.* **1991**, 1405–1407.
(21) Tremel, W. *Angew. Chem., Int. Ed. Engl.* **1991**, *30*, 840–843.
(22) Tremel, W. *Angew. Chem., Int. Ed. Engl.* **1992**, *31*, 217–220.
(23) Li, J.; Badding, M. E.; DiSalvo, F. J. *Inorg. Chem.* **1992**, *31*, 1050–1054.
(24) *Crystallography and Crystal Chemistry of Materials with Layered Structures*; Lévy, F., Ed.; Physics and Chemistry of Materials with Layered Structures 2; D. Reidel: Dordrecht, Holland, 1976.
(25) *Crystal Chemistry and Properties of Materials with Quasi-one-dimensional Structures*; Rouxel, J., Ed.; Physics and Chemistry of Materials with Low-dimensional Structures Series B; D. Reidel: Dordrecht, Holland, 1986.
(26) Wilson, J. A. *Phys. Rev. B* **1979**, *19*, 6456–6468.
(27) Wilson, J. A.; DiSalvo, F. J.; Mahajan, S. *Adv. Phys.* **1975**, *24*, 117–201.
(28) Ishihara, Y.; Nakada, I. *Solid State Commun.* **1983**, *45*, 129–132.
(29) Ishihara, Y.; Nakada, I.; Suzuki, K.; Ichihara, M. *Solid State Commun.* **1984**, *50*, 657–659.
(30) Suzuki, K.; Ichihara, M.; Nakada, I.; Ishihara, Y. *Solid State Commun.* **1984**, *52*, 743–746.
(31) DiSalvo, F. J.; Rice, T. M. *Phys. Today* **1979**, *32*, 32–38.
(32) *Electronic Properties of Inorganic Quasi-one-dimensional Compounds;* Monceau, P., Ed.; Physics and Chemistry of Materials with Low-dimensional Structures Series B; D. Reidel: Dordrecht, Holland, 1985; Parts 1 and 2.
(33) DiSalvo, F. J. *Surf. Sci.* **1976**, *58*, 297–311.
(34) Amberger, E.; Polborn, K.; Grimm, P.; Dietrich, M.; Obst, B. *Solid State Commun.* **1978**, *26*, 943–947.
(35) Biberacher, W.; Schwenk, H. *Solid State Commun.* **1980**, *33*, 385–387.
(36) Ishihara, Y.; Nakada, I. *Solid State Commun.* **1982**, *42*, 579–582.
(37) Fuller, W. W.; Chaikin, P. M.; Ong, N. P. *Solid State Commun.* **1979**, *30*, 689–692.
(38) Gamble, F. R.; DiSalvo, F. J.; Klemm, R. A.; Geballe, T. H. *Science* **1970**, *168*, 568–570.
(39) *Intercalated Layered Materials;* Lévy, F., Ed.; Physics and Chemistry of Materials with Layered Structures 6; D. Reidel: Dordrecht, Holland, 1979.
(40) Whittingham, M. S. *Prog. Solid State Chem.* **1978**, *12*, 41–99.
(41) Krönert, W.; Plieth, K. *Z. Anorg. Allg. Chem.* **1965**, *336*, 207–218.
(42) Furuseth, S.; Brattås, L.; Kjekshus, A. *Acta Chem. Scand., Ser A* **1975**, *29*, 623–631.
(43) Bjerkelund, E.; Kjekshus, A. *Acta Chem. Scand.* **1965**, *19*, 701–710.

0002-7863/93/1515-3227$04.00/0

electronic factors must also be considered when one assesses the probable existence of a compound. Encouraged by recent successful syntheses of ternary group IV metal–copper–telluride compounds (Cu_2MTe_3, M = Ti, Zr, Hf; $Cu_{1.85}Zr_2Te_6$),[9-11] we have extended our studies to include main-group metals as a second component. In the aforementioned compounds, copper typically resides in a tetrahedral site. Guided by the naive notion of linking coordination polyhedra together to formulate new target structures,[44-46] we attempted syntheses in the group IV metal–germanium–telluride systems, for Ge can also adopt tetrahedral coordination. Of course, its very different electronegativity and valency should lead to very different structures.

The only known ternary group IV metal germanium chalcogenides are the chalcogen-poor phases MGeQ (M = Zr, Hf; Q = S, Se, Te),[47,48] which adopt the PbFCl structure type. In these compounds, there is no ambiguity about the role that the Ge atoms play: they behave, together with the Q atoms, as anions that coordinate around the metal cation in a tricapped trigonal prismatic fashion. In the tellurium phases, MGeTe, one of the capping Te atoms is sufficiently distant that the metal atoms should properly be considered to be in a bicapped trigonal prismatic environment. The only known ternary group V metal germanium chalcogenide is the recently synthesized $Nb_3Ge_xTe_6$, $x = 1.0$,[19] $x \approx 0.9$.[18] Its structure contains Nb-centered trigonal prisms, whose rectangular faces are capped by Ge and neighboring Nb atoms. The Ge atoms in turn are coordinated by Te atoms in a distorted square-planar fashion. Thus, examination of these structures provides two important insights: (1) A bicapped trigonal prism, which is a ubiquitous feature in many ternary *group V* chalcogenides, can serve equally well as a structural unit in ternary *group IV* chalcogenides. (2) Because Ge abuts the line dividing metals and non-metals in the periodic table, it need not always be viewed as a cation, thereby permitting us to design hypothetical target structures in which it can play an anionic role. In chalcogen-rich systems, Ge will be more likely to serve as a cation. However, Te is hardly more electronegative (2.1) than Ge (2.0),[49,50] and we find in the tellurides that Ge participates in covalent bonding with both Te and the transition metal, M. Here, then, we report the syntheses of the new ternary tellurides $MGeTe_4$ (M = Zr, Hf) and $TiGeTe_6$. They crystallize in new layered structure types. In these phases, Ge may be viewed as serving as an anion by completing the coordination sphere of the metal and also as a cation in being coordinated in turn by three remaining Te atoms. While the Ge atoms are strictly four-coordinated, we find it more convenient to view them as trigonal pyramidally coordinated, with a "metal–metal" bond between Ge and the group IV metal. We illustrate the structural relationships between $MGeTe_4$ and $TiGeTe_6$ through the use of bicapped trigonal prisms and trigonal pyramids as the basic structural building blocks. Then we present electrical conductivity and magnetic susceptibility data for these compounds. Finally, we offer some insight into the bonding and physical properties in these compounds through the use of extended Hückel band-structure calculations.

Experimental Section

Syntheses. The starting materials were powders of the elements Ti (99.9%, AESAR), Zr (99.9%, Johnson-Matthey Electronics), Hf ("99.6%", but with Zr impurities at nominal levels of ~2%, Johnson-Matthey Electronics), Ge (99.999%, Johnson-Matthey Electronics), and Te (99.8%, Aldrich). In general, powders of the elements in various ratios (total weight 0.25 g) were ground together and loaded into quartz tubes (~10-cm length, 4-mm i.d.) that were then evacuated ($<10^{-4}$ Torr) and placed in a furnace. In the most successful heating profile for preparing the title compounds, the samples were heated to 650 °C over 1 day, kept at 650 °C for 1 day, heated to 900 °C over 6 h, kept at 900 °C for 4 days or longer, and slowly cooled to room temperature over 10 days. The products obtained were identified through microprobe analysis with an EDAX (energy dispersive analysis by X-rays) equipped Hitachi S570 scanning electron microscope and through X-ray powder diffraction patterns obtained on an Enraf-Nonius FR522 Guinier camera. Because of the layered nature of the structures, black crystals of the ternary compounds generally grow as flat needles that are very thin and easily bent. The compound $ZrGeTe_4$ is particularly prone to form as hairlike fibers. The products are invariably contaminated with binary compounds. Crystals of the ternary compounds usually grow in large aggregates or within a Te melt. Prolonged heating and slow cooling aid in providing better quality crystals, as does the use of an excess of Te, although it becomes more difficult to extract the crystals from the hard Te melt.

The samples used for the single-crystal X-ray structural studies of $ZrGeTe_4$, $HfGeTe_4$, and $TiGeTe_6$ were obtained from reactions of the elements in atomic ratios of Zr:Ge:Te = 1:1:4, Hf:Ge:Te = 1:1:4, and Ti:Ge:Te = 1:2:6, respectively. The samples used for the electrical conductivity and magnetic susceptibility measurements were obtained from reactions under diverse conditions (with use of at most a 2-fold excess of Te).

Structure Determination of $HfGeTe_4$. Analysis of rotation and Weissenberg photographs of $HfGeTe_4$ revealed Laue symmetry *mmm* and gave preliminary cell parameters. The systematic extinctions (*hkl*, $h + k = 2n + 1$; *h*0*l*, $l = 2n + 1$) are consistent with the orthorhombic space groups C_{2v}^{12}-*Cmc*2_1, C_{2v}^{17}-*C*2*cm*, and D_{2h}^{17}-*Cmcm*. The final cell parameters were determined from a least-squares analysis of the setting angles of 41 reflections in the range $18° < 2\theta(\text{Mo K}\alpha_1) < 41°$ that were automatically centered on a Picker diffractometer. Intensity data were collected at 113 K with the ω scan technique in the range $2° \le 2\theta(\text{Mo K}\alpha_1) \le 69°$ by methods standard in this laboratory.[51-53] Six standard reflections monitored at intervals of every 100 reflections showed no significant change during the data collection. Crystal data and further details of the data collection are given in Tables I and IS.[54]

All calculations were carried out on a Stardent ST2500 computer with methods and programs standard in this laboratory.[51] Conventional atomic

Table I Crystal Data and Intensity Collection for $HfGeTe_4$ and $TiGeTe_6$

	$HfGeTe_4$	$TiGeTe_6$
formula	$HfGeTe_4$	$TiGeTe_6$
formula mass, amu	761.50	886.09
space group	C_{2v}^{12}-*Cmc*2_1	C_{2h}^{3}-*C*2/*m*
a, Å	3.963(3)[a]	13.972(26)[a]
b, Å	15.875(10)	3.909(9)
c, Å	10.941(7)	17.454(32)
β, deg	-	104.95(5)
V, Å^3	688.3	921.0
Z	4	4
D(calcd), g cm^{-3}	7.35	6.39
T of data collection, K[b]	113	113
radiation	graphite monochromated Mo Kα (λ(Kα_1) = 0.7093 Å)	graphite monochromated Mo Kα (λ(Kα_1) = 0.7093 Å)
linear abs coeff, cm^{-1}	358.0	226.9
transmission factors[c]	0.611–0.714	0.685–0.893
$R(F^2)$	0.065	0.114
$R_w(F^2)$	0.081	0.121
R(on F for $F_o^2 > 3\sigma(F_o^2)$)	0.033	0.041

[a] The cell parameters for $HfGeTe_4$ and $TiGeTe_6$ were obtained from refinements constrained so that $\alpha = \beta = \gamma = 90°$ and $\alpha = \gamma = 90°$, respectively. [b] The low-temperature system is based on a design by Huffmann.[52] The diffractometer was operated with the use of the Indiana University PCPS system.[53] [c] The analytical method as employed in the Northwestern absorption program AGNOST was used for the absorption correction.[57]

(44) Keszler, D. A.; Ibers, J. A. *J. Am. Chem. Soc.* **1985**, *107*, 8119–8127.
(45) Sunshine, S. A.; Keszler, D. A.; Ibers, J. A. *Acc. Chem. Res.* **1987**, *20*, 395–400.
(46) Evain, M.; Brec, R. *Struct. Bonding* **1992**, *79*, 277–306.
(47) Onken, H.; Vierheilig, K.; Hahn, H. *Z. Anorg. Allg. Chem.* **1964**, *333*, 267–279.
(48) Haneveld, A. J. K.; Jellinek, F. *Recl. Trav. Chim. Pays-Bas* **1964**, *83*, 776–783.
(49) Emsley, J. *The Elements*; Clarendon Press: Oxford, England, 1989.
(50) Pauling, L. *The Nature of the Chemical Bond*, 3rd ed.; Cornell University Press: Ithaca, NY, 1960.
(51) Waters, J. M.; Ibers, J. A. *Inorg. Chem.* **1977**, *16*, 3273–3277.
(52) Huffmann, J. C. Ph.D. Dissertation, Indiana University, 1974.
(53) Huffmann, J. C. Unpublished work.
(54) Supplementary material.

and anomalous scattering factors were taken from the usual sources.[55,56] The intensity data were processed and corrected for absorption effects.[57] Of the 5829 measured reflections, those that were equivalent in space groups $Cmc2_1$, $C2cm$, and $Cmcm$ were averaged, resulting in R-indices for averaging of 0.10, 0.09, and 0.12 for 1690, 1574, and 881 reflections, respectively. The $|E|$ statistics favored the noncentrosymmetric space group $Cmc2_1$ or $C2cm$. Moreover, if we assume that the Hf atom must reside at a site of 4-fold multiplicity (affording a reasonable calculated density for $HfGeTe_4$), consideration of possible sites for the Te atoms that are consistent with the Patterson map eliminates $Cmcm$ and $C2cm$ as possible space groups. From the Patterson synthesis, the positions of the Hf and one of the Te atoms were located in space group $Cmc2_1$. The Ge and remaining Te atoms were located in subsequent electron density maps. The structure was then refined by least-squares methods, in which the function minimized was $\sum w(F_o^2 - F_c^2)$.[2]

The intensities of the unaveraged hkl and $hk\bar{l}$ reflections were compared in order to determine the sense of the polar axis z of this crystal. Of the 228 reflections for which F_c differed by more than 5% between the hkl and $hk\bar{l}$ reflections, 201 of the differences were accounted for by the chosen sense of the polar axis. The program STRUCTURE TIDY[58] was used to standardize the crystal structure according to rules formulated previously.[59] The program MISSYM[60] detected no additional symmetry elements beyond those expected in $Cmc2_1$, further supporting our choice of this space group. Because nonstoichiometry in transition-metal chalcogenides is sometimes observed,[10,44,61] a refinement (including anisotropic thermal parameters) was performed in which the Hf and Ge occupancies were allowed to vary while the Te occupancies were fixed. This procedure resulted in the formulation $Hf_{0.85(1)}Ge_{0.99(1)}Te_4$. With a fully stoichiometric model $HfGeTe_4$, the R-index is 0.040 and B_{eq} for the Hf atom is 0.77(2) Å^2. With the nonstoichiometric model $Hf_{0.85}GeTe_4$, the R-index improves slightly to 0.033 and B_{eq} for the Hf atom decreases to 0.44(2) Å^2, a value that is more comparable to those of the other atoms. Additional refinements in which the occupancies of successive atoms were fixed gave results that are consistent with a deficiency of Hf atoms in the chosen crystal. In the remainder of this paper we shall refer to this compound as "$HfGeTe_4$" with the understanding that it is probably nonstoichiometric and that the nature of this nonstoichiometry may well vary from crystal to crystal.

The final cycle of least-squares refinement on F_o^2 of 38 variables (including anisotropic thermal parameters and an isotropic extinction parameter) and 1690 averaged reflections (including those having $F_o^2 < 0$) converged to values of $R(F_o^2)$ of 0.065 and $R_w(F_o^2)$ of 0.081. The value for the conventional R-index (on F for $F_o^2 > 3\sigma(F_o^2)$) is 0.033 for 1239 reflections. The final difference electron density map shows no features with a height greater than 1% of that of a Hf atom ($\Delta\rho_{max}$ = 8.8; $\Delta\rho_{min}$ = −9.5 e Å^{-3}). No unusual trends were observed from an analysis of $\sum w(F_o^2 - F_c^2)^2$ as a function of F_o^2, $\lambda^{-1}\sin\theta$, and Miller indices. Final values of the positional parameters and equivalent isotropic thermal parameters are given in Table II. Anisotropic thermal parameters and final structure amplitudes are given in Tables IIS and IIIS, respectively.[54]

Unit Cell Determination of $ZrGeTe_4$. The similarity of the cell parameters and intensity patterns in the rotation and Weissenberg photographs of $ZrGeTe_4$ and $HfGeTe_4$ strongly suggests that these compounds are isostructural. The final cell parameters (a = 3.976(4), b = 15.876(16), and c = 10.948(12) Å) of a single crystal of $ZrGeTe_4$ were determined from a least-squares analysis of the setting angles of 28 centered reflections in the range 29° < 2θ(Mo Kα_1) < 42° on a Picker diffractometer at 113 K. In the following discussions, the formulation $MGeTe_4$ (M = Zr, Hf) shall refer to either of the two compounds and comments directed at one of these will generally apply to the other, given their close chemical and structural similarities.

Structure Determination of $TiGeTe_6$. Analysis of rotation and Weissenberg photographs of $TiGeTe_6$ revealed Laue symmetry $2/m$ and provided preliminary cell parameters. The systematic extinction (hkl, $h + k = 2n + 1$) is consistent with the monoclinic space groups C_2^3-$C2$, C_s^3-Cm, and C_{2h}^3-$C2/m$. The final cell parameters were determined from a least-squares analysis of the setting angles of 28 centered reflections in the range 14° < 2θ(Mo Kα_1) < 32°. Intensity data were collected at 113 K with the ω scan technique in the range 2° ≤ 2θ(Mo Kα_1) ≤ 52°. The fragile nature of these crystals, which are easily bent, leads to generally poor crystal quality. The broadening of the peaks necessitated a wide scan range (4.0° in ω). Six standard reflections monitored at intervals of every 100 reflections were stable during the course of data collection. Crystal data and further details of the data collection are given in Tables I and IS.[54]

After the 3600 measured reflections were processed and corrected for absorption effects, those that were equivalent in space groups $C2/m$, Cm, and $C2$ were averaged, resulting in R-indices for averaging of 0.17, 0.17, and 0.15 for 1046, 2087, and 1809 unique data, respectively. As there is no strong support for the noncentrosymmetric space groups, we chose the space group $C2/m$, for which refinement proceeded satisfactorily. The initial positions for all atoms were determined by direct methods with the program SHELXS86,[62] and the structure was refined by least-squares methods. The program STRUCTURE TIDY[58] was used to standardize the crystal structure. The program MISSYM[60] found no additional symmetry elements beyond those expected in $C2/m$. In order to test for nonstoichiometry in this crystal, a refinement was performed in which the Ti and Ge occupancies were allowed to vary while the Te occupanices were fixed. This resulted in a stoichiometry $Ti_{1.01(2)}Ge_{0.99(2)}Te_6$ with reasonable thermal parameters for all atoms. Thus, we accept the stoichiometric formulation $TiGeTe_6$. The final cycle of least-squares refinement on F_o^2 of 50 variables (including anisotropic thermal parameters and an isotropic extinction parameter) and 1046 averaged reflections (including those having $F_o^2 < 0$) converged to values of $R(F_o^2)$ of 0.114 and $R_w(F_o^2)$ of 0.121. The value for the conventional R-index (on F for $F_o^2 > 3\sigma(F_o^2)$) is 0.041 for 501 reflections. The final difference electron density map shows no features with a height greater than 4% of that of a Te atom ($\Delta\rho_{max}$ = 7.5; $\Delta\rho_{min}$ = −7.6 e Å^{-3}). No unusual trends were observed from an analysis of $\sum w(F_o^2 - F_c^2)^2$ as a function of F_o^2, $\lambda^{-1}\sin\theta$, and Miller indices. Final values of the positional parameters and equivalent isotropic thermal parameters are given in Table II. Anisotropic thermal parameters and final structure amplitudes are given in Tables IIS and IIIS, respectively.[54] Upon discovery that $TiGeTe_6$ appears to undergo a metal-to-semiconductor transition at ~165 K (vide infra), the cell parameters of the same crystal used for the structure determination were remeasured as a function of temperature. Within their standard deviations, the cell parameters showed no abrupt change between 113 K (a = 13.98(1), b = 3.885(3), c = 17.44(2) Å; β = 104.83(6)°) and 198 K (a = 13.98(2), b = 3.887(4), c = 17.48(3) Å, β = 104.77(6)°).

Electrical Conductivity. Single crystals of $ZrGeTe_4$, $HfGeTe_4$, and $TiGeTe_6$ ranging in length from 0.9 to 1.4 mm were mounted with Ag

Table II. Positional Parameters and Equivalent Isotropic Thermal Parameters for $HfGeTe_4$ and $TiGeTe_6$

atom	x	y	z	B_{eq}, Å^2 [a]
		$HfGeTe_4$[c]		
Hf[b]	0	0.151 767(47)	0	0.44(2)
Ge	0	0.727 92(11)	0.310 64(16)	0.54(3)
Te(1)	0	0.118 708(65)	0.272 48(11)	0.47(2)
Te(2)	0	0.222 025(65)	0.576 12(11)	0.46(2)
Te(3)	0	0.399 059(65)	0.311 84(11)	0.50(2)
Te(4)	0	0.516 014(63)	0.029 50(12)	0.55(2)
		$TiGeTe_6$[d]		
Ti	0.735 69(50)	0	0.258 18(32)	1.1(2)
Ge	0.280 70(30)	0	0.593 93(20)	1.1(1)
Te(1)	0.083 21(18)	0	0.253 98(12)	0.99(7)
Te(2)	0.122 88(20)	0	0.464 40(13)	0.96(6)
Te(3)	0.153 09(19)	0	0.015 42(12)	1.17(7)
Te(4)	0.319 75(19)	0	0.178 35(13)	1.15(7)
Te(5)	0.374 22(19)	0	0.345 13(12)	1.11(7)
Te(6)	0.587 33(19)	0	0.113 61(13)	1.12(7)

[a] $B_{eq} = (8\pi^2/3)\sum_i\sum_j U_{ij}a_i^*a_j^*\mathbf{a}_i\cdot\mathbf{a}_j$. [b] Occupancy = 0.85(1). [c] All atoms are in Wyckoff position 4a. [d] All atoms are in Wyckoff position 4i.

(55) Cromer, D. T.; Waber, J. T. In *International Tables for X-ray Crystallography*; Ibers, J. A., Hamilton, W. C., Eds.; Kynoch Press: Birmingham, England, 1974; Vol. IV, pp 72–98.
(56) Cromer, D. T. In *International Tables for X-ray Crystallography*; Ibers, J. A., Hamilton, W. C., Eds.; Kynoch Press: Birmingham, England, 1974; Vol. IV, pp 149–150.
(57) de Meulenaer, J.; Tompa, H. *Acta Crystallogr.* **1965**, *19*, 1014–1018.
(58) Gelato, L. M.; Parthé, E. *J. Appl. Crystallogr.* **1987**, *20*, 139–143.
(59) Parthé, E.; Gelato, L. M. *Acta Crystallogr., Sect. A: Found. Crystallogr.* **1984**, *40*, 169–183.
(60) Le Page, Y. *J. Appl. Crystallogr.* **1987**, *20*, 264–269.
(61) Squattrito, P. J.; Swepston, P. N.; Ibers, J. A. *Inorg. Chem.* **1987**, *26*, 1187–1188.
(62) Sheldrick, G. M. In *Crystallographic Computing 3*; Sheldrick, G. M., Krüger, C., Goddard, R., Eds.; Oxford University Press: London, 1985; pp 175–189.

Table III. Extended Hückel Parameters[a]

atom	orbital	H_{ii}, eV	ζ_1	c_1[b]	ζ_2	c_2[b]
Zr[c]	5s	−8.00	1.82			
	5p	−5.40	1.78			
	4d	−10.20	3.84	0.6224	1.50	0.5782
Ti[d]	4s	−8.90	1.82			
	4p	−5.40	1.30			
	3d	−11.20	4.55	0.4391	1.60	0.7397
Ge[e]	4s	−16.0	2.16			
	4p	−9.0	1.85			
Te[f]	5s	−20.80	2.51			
	5p	−13.20	2.16			

[a] A modified Wolfsberg–Helmholz formula was used to calculate the off-diagonal H_{ij} values.[71] [b] Contraction coefficients used in the double-ζ expansion. [c] References 11, 72, and 73. [d] Reference 74. [e] Reference 75. [f] References 11, 17, 73, 74, and 76.

paint on Au wires, extended by graphite fibers, of an integrated circuit chip can. The integrity of the mounted crystals was verified by EDAX measurements. The electrical conductivities along the needle axes *a* of $ZrGeTe_4$ and $HfGeTe_4$, and *b* of $TiGeTe_6$ were measured by a four-probe ac (27 Hz) phase-locked technique, similar to a procedure described previously.[63] Samples were cooled at a rate of 1–2° min^{-1} by use of a flow of He gas. The temperature was measured with a LakeShore DT-470 silicon diode temperature sensor located close to the crystal. The uncertainties in the measurements of the crystal dimensions, particularly of the cross-sectional area, led to relative uncertainties in the conductivity values of $(\Delta\sigma)/\sigma = \pm 0.2$. Generally, the cross-sectional areas of the crystals examined were on the order of 10^{-4} mm^2. Clearly, these crystals are too thin to permit measurements of conductivity perpendicular to the needle axes.

Magnetic Susceptibility. Single crystals or aggregates of single crystals were manually selected from various reactions. X-ray powder diffraction on representative portions of crushed crystals confirmed that the samples of $HfGeTe_4$ and $TiGeTe_6$ were phase pure. However, the $ZrGeTe_4$ sample was contaminated with considerable amounts of $ZrTe_3$ and $ZrTe_5$ (whose crystal habits are virtually indistinguishable from that of $ZrGeTe_4$). We estimate the sample to be ~70% pure, at best. The compounds $ZrTe_3$ and $ZrTe_5$ are diamagnetic with room-temperature susceptibilities of -3.6×10^{-7} and -4.3×10^{-7} emu g^{-1}, respectively.[64,65] No attempt was made to correct for their contributions to the measured susceptibility of the $ZrGeTe_4$ sample.

Band-Structure Calculations. One-electron band-structure calculations were performed by the tight-binding method with an extended Hückel type Hamiltonian.[66-71] The atomic parameters used[11,17,72-76] are listed in Table III. Although it is the crystal structure of $HfGeTe_4$ that we have determined, we performed the band-structure calculation on $ZrGeTe_4$ instead, as we were unable to locate *reliable* Hückel parameters for Hf while those for Zr appear to be well entrenched on the basis of several previous calculations.[11,72,73] We feel that this procedure is justified because the cell parameters for the two compounds are essentially equal and the atomic radii for Zr and Hf are identical.[77] Therefore, we have taken the atomic coordinates of $HfGeTe_4$ for the band-structure calculation of $ZrGeTe_4$. We have also chosen not to reduce the *C*-centered orthorhombic unit cell so that the symmetry of the crystal structure may be preserved, thereby permitting us to relate special lines in the Brillouin zone with the conduction and stacking directions of the crystal structure. Nor have we reduced the *C*-centered monoclinic cell of $TiGeTe_6$. Essentially, this procedure results in degeneracies at high-symmetry points and folding of bands in the band dispersion diagrams, but the density of states (DOS) and the crystal orbital overlap populations (COOP) are unaffected. Properties extracted from the band structures were calculated with the use of a mesh size of 96 and 72 *k*-points,[78] respectively, in the irreducible portion of the Brillouin zone in $ZrGeTe_4$ and $TiGeTe_6$. A Gaussian smoothing factor of 0.10 was used for 300 mesh points between −18.0 and −2.0 eV in the DOS and COOP plots.

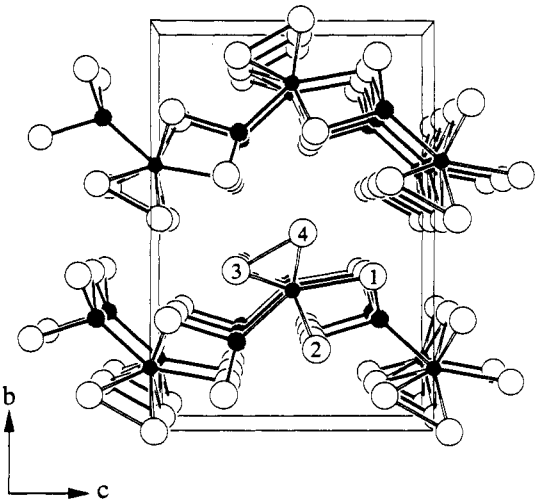

Figure 1. View down the *a* axis of $HfGeTe_4$ showing the labeling scheme and unit cell outline. The small solid circles are Hf atoms, the medium hatched circles are Ge atoms, and the large open circles are Te atoms.

Results and Discussion

1. Description of the Structures. The structures of $HfGeTe_4$ and $TiGeTe_6$ are closely related to each other and to those of some binary chalcogenides. We describe the structure of $HfGeTe_4$, the simpler of the two, before that of $TiGeTe_6$ and then proceed to a discussion of their structural interrelationships.

A view of the structure of $HfGeTe_4$ down the *a* axis is given in Figure 1, which shows the labeling scheme. The compound $HfGeTe_4$ possesses a new layered structure type that comprises layers of composition $^{2}_{\infty}[HfGeTe_4]$ lying parallel to the (010) plane. A view down the *b* axis, showing part of a single layer, is given in Figure 2. This layer can be decomposed into one-dimensional columns of polyhedra. The Hf atoms are surrounded by six Te atoms in a trigonal prismatic fashion. The atoms Te(2), Te(3), and Te(4) form a triangle that is isosceles rather than equilateral, the Te(3)–Te(4) distance (2.737(2) Å) being considerably shorter than the other two (>4.0 Å). The Hf atoms are further coordinated by a Te(1) atom and a Ge atom that cap two of the rectangular faces of the trigonal prism. Thus, the geometry around the Hf atom is properly described as bicapped trigonal prismatic. The Hf bicapped trigonal prisms then share their triangular faces to form one-dimensional chains $^{1}_{\infty}[HfGeTe_4]$ along the direction of the *a* axis. The Ge atoms are surrounded by three Te atoms (Te(2) and two Te(1)) in a trigonal pyramidal fashion and by a Hf atom. Thus, the Ge atom resides in a distorted tetrahedral environment. The Ge tetrahedra then share their corners (through atom Te(1)) to form one-dimensional chains $^{1}_{\infty}[GeHfTe_2]$. If we adhere strictly to the usual conventions of a polyhedral representation,[79,80] then we find it difficult

(63) Phillips, T. E.; Anderson, J. R.; Schramm, C. J.; Hoffman, B. M. *Rev. Sci. Instrum.* **1979**, *50*, 263–265.
(64) Brattås, L.; Kjekshus, A. *Acta Chem. Scand.* **1972**, *26*, 3441–3449.
(65) DiSalvo, F. J.; Fleming, R. M.; Waszczak, J. V. *Phys. Rev. B: Condens. Matter* **1981**, *24*, 2935–2939.
(66) Whangbo, M.-H.; Hoffmann, R. *J. Am. Chem. Soc.* **1978**, *100*, 6093–6098.
(67) Hoffmann, R. *Angew. Chem., Int. Ed. Engl.* **1987**, *26*, 846–878.
(68) Whangbo, M.-H.; Hoffmann, R.; Woodward, R. B. *Proc. R. Soc. London, A* **1979**, *366*, 23–46.
(69) Hoffmann, R. *J. Chem. Phys.* **1963**, *39*, 1397–1412.
(70) Hoffmann, R. *Solids and Surfaces: A Chemist's View of Bonding in Extended Structures*; VCH Publishers: New York, 1988.
(71) Ammeter, J. H.; Bürgi, H.-B.; Thibeault, J. C.; Hoffmann, R. *J. Am. Chem. Soc.* **1978**, *100*, 3686–3692.
(72) Canadell, E.; Whangbo, M.-H. *Inorg. Chem.* **1990**, *29*, 1398–1401.
(73) Canadell, E.; Mathey, Y.; Whangbo, M.-H. *J. Am. Chem. Soc.* **1988**, *110*, 104–108.
(74) Canadell, E.; Jobic, S.; Brec, R.; Rouxel, J.; Whangbo, M.-H. *J. Solid State Chem.* **1992**, *99*, 189–199.
(75) Thorn, D. L.; Hoffmann, R. *Inorg. Chem.* **1978**, *17*, 126–140.
(76) Canadell, E.; Jobic, S.; Brec, R.; Rouxel, J. *J. Solid State Chem.* **1992**, *98*, 59–70.
(77) Shannon, R. D. *Acta Crystallogr., Sect. A: Cryst. Phys., Diffr., Theor. Gen. Crystallogr.* **1976**, *32*, 751–767.
(78) Ramírez, R.; Böhm, M. C. *Int. J. Quantum Chem.* **1986**, *30*, 391–411.
(79) Smith, J. V. *Geometrical and Structural Crystallography*; Wiley: New York, 1982.

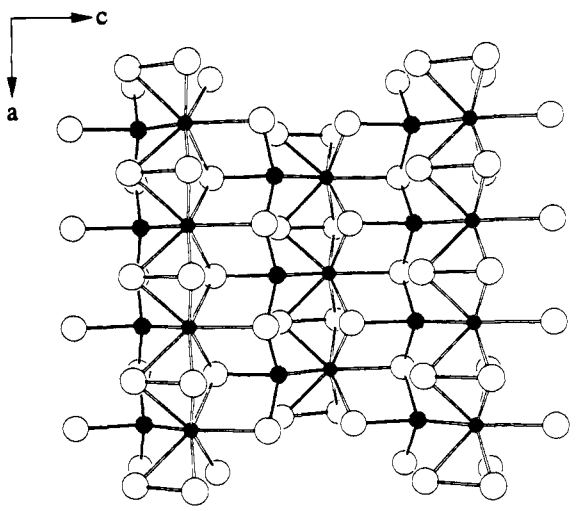

Figure 2. View down the *b* axis of $HfGeTe_4$ showing an individual layer and the one-dimensional polyhedral chains extending along the *a* direction. Atoms are as marked in Figure 1.

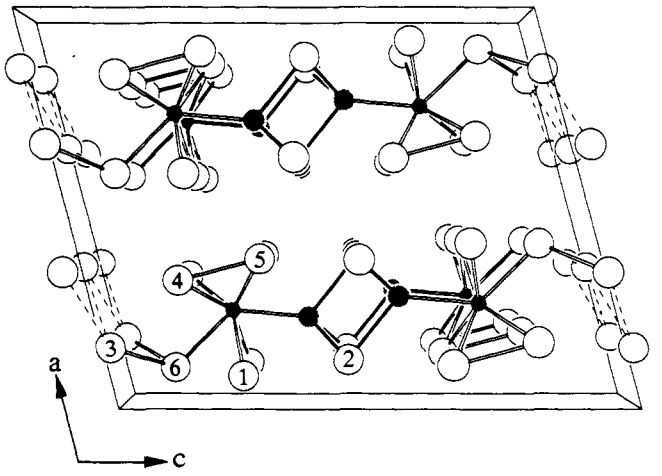

Figure 3. View down the *b* axis of $TiGeTe_6$ showing the labeling scheme and unit cell outline. The small solid circles are Ti atoms, the medium hatched circles are Ge atoms, and the large open circles are Te atoms.

to describe this structure because the center of one polyhedron (Ge) also serves as a vertex for an adjacent polyhedron (Hf bicapped trigonal prism). We shall shortly present alternative ways of looking at the structure, but it is clear from Figure 2 that a layer of $HfGeTe_4$ is formed from the linking of one-dimensional chains. The layers are then stacked to form the three-dimensional structure in the manner shown in Figure 1.

A view of the structure of $TiGeTe_6$ down the *b* axis is given in Figure 3, which shows the labeling scheme. The compound $TiGeTe_6$ also presents a new structure type. Whether it is a true two-dimensional structure or a one-dimensional structure (as suggested by the dotted lines joining the Te(3) atoms to symmetry-related ones in the next unit cell) is a matter we shall address below. For the moment, we regard the structure as consisting of chains of composition $^1_\infty[Ti_2Ge_2Te_{12}]$ that span a *c*-parameter repeat and lie parallel to the (100) plane. A view down the *a* axis, showing part of such a chain, is given in Figure 4. The Ti atoms are initially viewed as being coordinated by six Te atoms in a trigonal prismatic environment, the Te(4), Te(5), and Te(1) atoms forming the isosceles triangular faces and the Te(4)–Te(5) link (2.812(6) Å) forming the short side. The Te(6) and Ge atoms cap two rectangular faces of the trigonal prism to complete the bicapped trigonal prismatic cooordination of the Ti atoms. One-

(80) Wells, A. F. *Structural Inorganic Chemistry*, 5th ed.; Clarendon Press: Oxford, England, 1984.

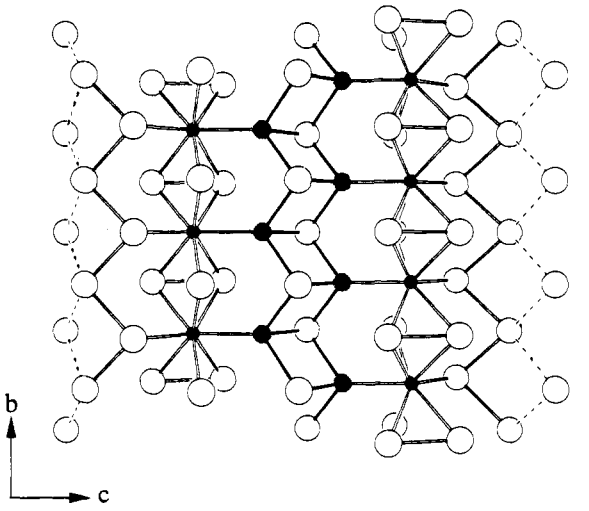

Figure 4. View perpendicular to the (100) plane of $TiGeTe_6$ showing an individual $^1_\infty[Ti_2Ge_2Te_{12}]$ chain and the one-dimensional polyhedral chains extending along the *b* direction. Atoms are as marked in Figure 3. The dotted lines indicate that the $^1_\infty[Ti_2Ge_2Te_{12}]$ chains are linked to one another to form a layer in $TiGeTe_6$.

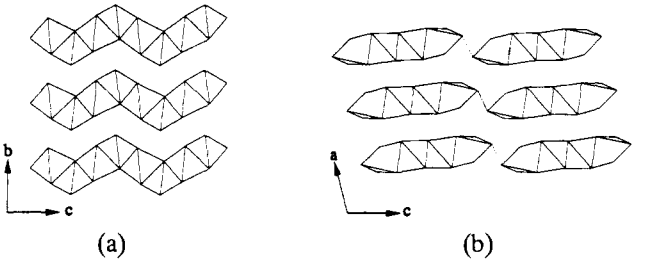

Figure 5. Simplified representations of several layers in (a) $HfGeTe_4$ and (b) $TiGeTe_6$ illustrating the appearance of the van der Waals gaps.

dimensional chains $^1_\infty[TiGeTe_4]$ running along the *b*-axis direction form when the bicapped trigonal prisms share their triangular faces. The Ge atoms are coordinated by a Ti and three Te(2) atoms, forming corner-shared tetrahedra $^1_\infty[GeTiTe_2]$ running down the *b*-axis direction. By sharing edges, two such single chains are joined together to form a double tetrahedral chain. The trigonal prismatic and tetrahedral chains are condensed together, and finally the $^1_\infty[Ti_2Ge_2Te_{12}]$ chain is completed by having its ends bordered by zigzag Te(3)–Te(6) chains. The $^1_\infty[Ti_2Ge_2Te_{12}]$ units are linked together (Te(3)···Te(3)) along the *c*-axis direction to form a two-dimensional layer $^2_\infty[Ti_2Ge_2Te_{12}]$. These layers then stack to form the three-dimensional structure shown in Figure 3.

Although the structural building blocks in $HfGeTe_4$ and $TiGeTe_6$ show some interesting similarities, their different arrangement leads to very different layered structures. One gross difference is the nature of the van der Waals gap. As shown in Figure 5, the van der Waals gap is undulated in $HfGeTe_4$, while it is obviously more planar in $TiGeTe_6$. Because the Te atoms are not close-packed in the sheets, the van der Waals gap in $TiGeTe_6$ remains slightly buckled and irregular.

Selected interatomic distances and angles for $HfGeTe_4$ and $TiGeTe_6$ are given in Tables IV and V, respectively. For ease of comparison, some relevant distances in $HfGeTe_4$ and $TiGeTe_6$ are presented in their molecular fragments, as shown in Figure 6.

The Hf–Te distances (2.938(2)–3.027(2) Å) are consistent with similar distances in Cu_2HfTe_3 (2.736(1)–3.053(1) Å),[9] $K_4Hf_3Te_{17}$ (2.900(4)–3.054(4) Å),[8] and $HfTe_5$ (2.954(3)–2.960(2)

Table IV. Selected Interatomic Distances (Å) and Angles (deg) for $HfGeTe_4$

Hf–Ge	2.818(2)	Te(1)–2Te(4)	3.695(2)
Hf–2Te(2)	2.938(2)	Te(1)–Te(2)	3.705(2)
Hf–2Te(4)	2.945(2)	Te(1)–2Te(2)	3.864(2)
Hf–2Te(3)	2.969(2)	Te(1)–2Te(1)	3.963(3)
Hf–Te(1)	3.027(2)	Te(2)–2Te(3)	3.778(2)
Hf–2Hf	3.963(3)	Te(2)–2Te(2)	3.963(3)
Ge–2Te(1)	2.666(2)	Te(3)–Te(4)	2.737(2)
Ge–Te(2)	2.686(2)	Te(3)–Te(4)	3.604(2)
Ge–2Ge	3.963(3)	Te(3)–2Te(3)	3.963(3)
		Te(4)–2Te(4)	3.963(3)
Ge–Hf–Te(1)	147.31(5)	Te(2)–Hf–Te(4)	90.81(6)
Ge–Hf–Te(2)	75.30(5)	Te(3)–Hf–Te(3)	83.73(6)
Ge–Hf–Te(3)	71.00(5)	Te(3)–Hf–Te(4)	55.12(4)
Ge–Hf–Te(4)	125.21(4)	Te(4)–Hf–Te(4)	84.56(7)
Te(1)–Hf–Te(2)	80.74(4)	Hf–Ge–Te(1)	123.78(5)
Te(1)–Hf–Te(3)	129.48(4)	Hf–Ge–Te(2)	120.12(8)
Te(1)–Hf–Te(4)	76.42(3)	Te(1)–Ge–Te(1)	96.02(9)
Te(2)–Hf–Te(2)	84.81(6)	Te(1)–Ge–Te(2)	92.45(5)
Te(2)–Hf–Te(3)	86.09(5)		

Table V. Selected Interatomic Distances (Å) and Angles (deg) for $TiGeTe_6$

Ti–Ge	2.650(8)	Te(1)–2Te(1)	3.909(9)
Ti–Te(6)	2.822(8)	Te(1)–Te(5)	3.966(8)
Ti–2Te(4)	2.826(6)	Te(2)–2Te(5)	3.848(6)
Ti–2Te(1)	2.878(7)	Te(2)–2Te(2)	3.909(9)
Ti–2Te(5)	2.890(6)	Te(2)–Te(2)	3.942(8)
Ti–2Ti	3.909(9)	Te(2)–2Te(2)	3.963(8)
Ge–2Te(2)	2.716(5)	Te(3)–2Te(6)	2.901(4)
Ge–Te(2)	2.720(6)	Te(3)–Te(4)	3.177(6)
Ge–2Ge	3.722(8)	Te(3)–2Te(3)	3.492(6)
Ge–2Ge	3.909(9)	Te(3)–2Te(3)	3.909(9)
		Te(4)–Te(5)	2.812(6)
Te(1)–2Te(6)	3.146(5)	Te(4)–2Te(6)	3.708(6)
Te(1)–Te(2)	3.570(7)	Te(4)–2Te(4)	3.909(9)
Te(1)–Te(4)	3.862(7)	Te(5)–2Te(5)	3.909(9)
		Te(6)–2Te(6)	3.909(9)
Ge–Ti–Te(6)	130.0(3)	Te(5)–Ti–Te(4)	58.9(2)
Ge–Ti–Te(1)	77.0(2)	Te(4)–Ti–Te(4)	87.5(2)
Ge–Ti–Te(5)	72.7(2)	Ti–Ge–Te(2)	122.7(1)
Ge–Ti–Te(4)	129.2(2)	Ti–Ge–Te(2)	123.7(2)
Te(6)–Ti–Te(1)	67.0(2)	Te(2)–Ge–Te(2)	92.0(2)
Te(6)–Ti–Te(5)	135.0(1)	Te(2)–Ge–Te(2)	93.6(2)
Te(6)–Ti–Te(4)	82.1(2)		
Te(1)–Ti–Te(1)	85.5(3)	Te(6)–Te(3)–Te(6)	84.7(2)
Te(1)–Ti–Te(5)	86.9(2)	Ti–Te(6)–Te(3)	104.9(2)
Te(1)–Ti–Te(4)	85.2(2)		
Te(5)–Ti–Te(5)	85.1(2)		

Å).[81,82] The latter two compounds also contain Hf in bicapped trigonal prismatic environments. To our knowledge, $TiGeTe_6$ provides the only example of Ti in a bicapped trigonal prismatic coordination by Te, so that proper comparisons of Ti–Te bond distances are not easy. The Ti–Te distances (2.822(8)–2.890(6) Å) in $TiGeTe_6$ are longer than that in $TiTe_2$ (2.770(2) Å)[83] and intermediate between those in Ti_5Te_4 (2.773(10)–2.905(2) Å).[84]

The Ge–Te distances in $HfGeTe_4$ (2.666(2)–2.686(2) Å) and $TiGeTe_6$ (2.716(5)–2.720(6) Å) are shorter than that in GeTe (2.843 Å)[85-87] but generally longer than those in a number of ternary alkali-metal germanium tellurides (e.g.: $Na_6Ge_2Te_6$, 2.568(1)–2.572(1) Å;[88] $K_6Ge_2Te_6$, 2.564(4)–2.590(5) Å;[89] $Ba_2Ge_2Te_5$, 2.557(4)–2.644(4) Å[90]). In all these Ge-containing

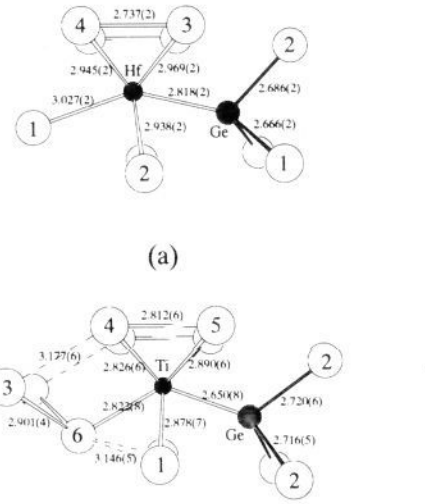

Figure 6. Selected distances in molecular fragments of (a) $HfGeTe_4$ and (b) $TiGeTe_6$.

compounds, the Ge atom bonds to three Te atoms and (except in GeTe) another Ge, Hf, or Ti atom. The Te–Ge–Te angles in $HfGeTe_4$ (92.45(5)–96.02(9)°) and $TiGeTe_6$ (92.0(2)–93.6(2)°) are closer to the trigonal pyramidal angle in GeTe (94.16°)[85-87] than the tetrahedral angles in the alkali-metal germanium tellurides (e.g.: $Na_6Ge_2Te_6$, 107.0(1)–108.8(1)°;[88] $K_6Ge_2Te_6$, 109.1(2)–109.4(2)°;[89] $Ba_2Ge_2Te_5$, 96.1(1)–122.9(1)° [90]). In $Nb_3Ge_xTe_6$, the Ge atom bonds in a square-planar fashion to four Te atoms at distances (x = 1.0, 2.762(2)–2.803(2) Å[19] or $x \approx 0.9$, 2.745(1)–2.790(1) Å[18]) longer than those in $HfGeTe_4$ and $TiGeTe_6$.

The metal–Ge bonds are an interesting feature in $HfGeTe_4$ and $TiGeTe_6$. The Hf–Ge distance in $HfGeTe_4$ (2.818(2) Å) compares well with those found in some metal germanides (HfGeTe, 2.82 Å;[47] $HfGe_2$, 2.78–3.13 Å;[91] Hf_2CuGe_4, 2.72–2.85 Å[92]). When the smaller ionic radius for eight-coordinated Ti^{4+} (0.74 Å) vs Hf^{4+} (0.83 Å)[77] is taken into account, the Ti–Ge distance in $TiGeTe_6$ (2.650(8) Å) is shorter and is within the range found in Ti_6Ge_5 (2.50–2.95 Å).[93]

A wide range of Te–Te distances is observed in the present compounds. In $HfGeTe_4$, the Te(3)–Te(4) distance (2.737(2) Å) is short and is indicative of a Te–Te single bond (cf. 2.763(4) Å in $HfTe_5$).[81] The other Te–Te distances range from 3.604(2) Å (the shortest interlayer Te–Te distance) to 3.963(3) Å within the layers. Although these distances are less than an ionic Te^{2-}–Te^{2-} separation (~4 Å),[77] the presence of any weak bonding interactions must also be evaluated through their overlap populations (vide infra). In $TiGeTe_6$, there are two short Te–Te distances (Te(4)–Te(5), 2.812(6) Å; Te(3)–Te(6), 2.901(4) Å) indicative of a single bond, two slightly longer distances (Te(1)–Te(6), 3.146(5) Å; Te(3)–Te(4), 3.177(6) Å) that are also likely to be bonding, and a Te(3)–Te(3) distance (3.492(6) Å) that provides the weak link between the $^1_\infty[Ti_2Ge_2Te_{12}]$ chains to form the two-dimensional layer. The van der Waals separation is large, the shortest interlayer distance (Te(2)–Te(2)) being 3.942(8) Å.

(81) Furuseth, S.; Brattås, L.; Kjekshus, A. *Acta Chem. Scand.* **1973**, *27*, 2367–2374.
(82) Fjellvåg, H.; Kjekshus, A. *Solid State Commun.* **1986**, *60*, 91–93.
(83) Arnaud, Y.; Chevreton, M. *J. Solid State Chem.* **1981**, *39*, 230–239.
(84) Gronvold, F.; Kjekshus, A.; Raaum, F. *Acta Crystallogr.* **1961**, *14*, 930–934.
(85) Chattopadhyay, T.; Boucherle, J. X.; von Schnering, H. G. *J. Phys. C: Solid State Phys.* **1987**, *20*, 1431–1440.
(86) Goldak, J.; Barrett, C. S.; Innes, D.; Youdelis, W. *J. Chem. Phys.* **1966**, *44*, 3323–3325.
(87) Schubert, K.; Fricke, H. *Z. Metallkd.* **1953**, *44*, 457–461.
(88) Eisenmann, B.; Kieselbach, E.; Schäfer, H.; Schrod, H. *Z. Anorg. Allg. Chem.* **1984**, *516*, 49–54.
(89) Dittmar, G. *Z. Anorg. Allg. Chem.* **1978**, *453*, 68–78.
(90) Brinkmann, C.; Eisenmann, B.; Schäfer, H. *Z. Anorg. Allg. Chem.* **1984**, *517*, 143–148.
(91) Smith, J. F.; Bailey, D. M. *Acta Crystallogr.* **1957**, *10*, 341–342.
(92) Thirion, F.; Venturini, G.; Malaman, B.; Steinmetz, J.; Roques, B. *J. Less-Common Met.* **1983**, *95*, 47–54.
(93) Hallais, J. *Ann. Chim. (Paris)* **1971**, *6*, 321–330.

Scheme I

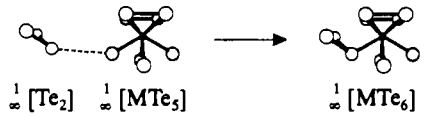

Scheme II

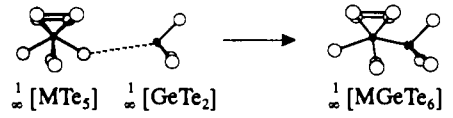

Scheme III

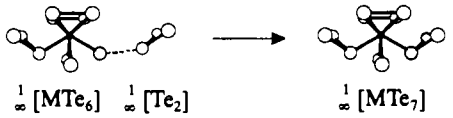

Scheme IV

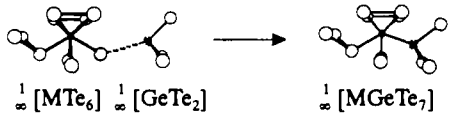

Scheme V

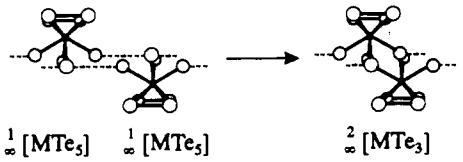

From a comparison of the interatomic distances in $HfGeTe_4$ and $TiGeTe_6$ with those of related compounds where oxidation states have been established, we suggest the formal charge balances represented by $M^{4+}Ge^{2+}(Te_2^{2-})(Te^{2-})_2$ (M = Zr, Hf) and $Ti^{4+}Ge^{2+}(Te_2^{2-})_2(Te^{-})_2$. However, consideration of the electronic structures (vide infra) will result in modification of these assignments of oxidation states.

2. Structural Interrelationships. It is always informative to try to relate an unfamiliar or new structure to known or simpler structures. In describing an extended structure, we prefer to decompose it, when possible, into an association of polyhedra.[44,79] Not only is this approach useful in the organization and classification of diverse structures, but it also brings us back to the molecule, as has been so poetically expressed, "the heart of chemistry".[70] While classical solid-state structures, especially oxides, are usually composed of octahedra and tetrahedra,[79,80] here we take two less familiar polyhedra, a bicapped trigonal prism and a trigonal pyramid, and construct and relate various structures.

The schemes provide simplified representations of these structural units, which are envisioned to be extended perpendicular to the plane of the page, hence the notation. Thus, in Schemes I and II, we see zigzag $^1_\infty[Te_2]$ chains, face-sharing bicapped trigonal prismatic $^1_\infty[MTe_5]$ chains, and corner-sharing trigonal pyramidal $^1_\infty[GeTe_2]$ chains. Successive replacement of the capping atoms of the bicapped trigonal prisms by zigzag $^1_\infty[Te_2]$ chains or $^1_\infty[GeTe_2]$ trigonal pyramidal chains (or both) produces the more complex building blocks in Schemes I–IV.

Condensation of $^1_\infty[MTe_5]$ bicapped trigonal prismatic chains through their capping atoms (Scheme V) produces the two-dimensional layer $^2_\infty[MTe_3]$, the structure adopted by the group IV trichalcogenides TiS_3 and MQ_3 (M = Zr, Hf; Q = S, Se, Te).[42] Interestingly, $TiSe_3$ and $TiTe_3$ have not been made.[42,94]

(94) McTaggart, F. K.; Wadsley, A. D. *Aust. J. Chem.* **1958**, *11*, 445–457.

Scheme VI

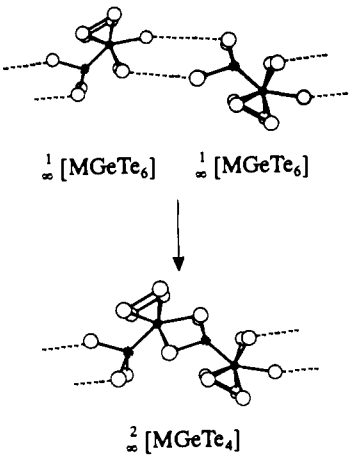

Scheme VII

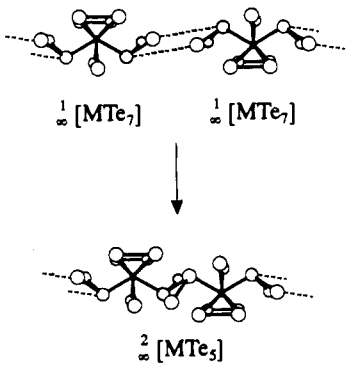

Scheme VIII

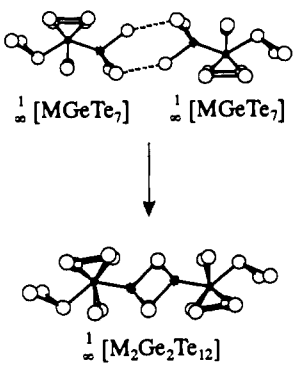

Condensation of the Ge-capping $^1_\infty[MGeTe_6]$ bicapped trigonal prismatic chains (Scheme VI) produces the layer $^2_\infty[MGeTe_4]$ found in $ZrGeTe_4$ and $HfGeTe_4$. Note that $MGeTe_4$ differs from MTe_3 only in the insertion of $^1_\infty[GeTe_2]$ chains between the trigonal prisms.

Similarly, condensation of the two-armed $^1_\infty[MTe_7]$ chains (Scheme VII) produces the layer $^2_\infty[MTe_5]$ that is found in $ZrTe_5$ and $HfTe_5$.[81,82,95,96] Condensation of *two* Ge-capping $^1_\infty[MGeTe_7]$ bicapped trigonal prismatic chains (Scheme VIII) produces the one-dimensional chain $^1_\infty[M_2Ge_2Te_{12}]$ found in $TiGeTe_6$. By weak association of such chains through a ~3.5-Å Te–Te contact, the two-dimensional layers in $TiGeTe_6$ are formed. The difference in MTe_5 and $TiGeTe_6$ is in the entities holding the trigonal prisms together: a Te zigzag chain in the former and a double Ge chain in the latter. In view

(95) Sambongi, T.; Biljakovic, K.; Smontara, A.; Guemas, L. *Synth. Met.* **1985**, *10*, 161–168.

(96) Eaglesham, D. J.; Mulcahy, J.; Wilson, J. A. *J. Phys. C: Solid State Phys.* **1987**, *20*, 351–355.

Scheme IX

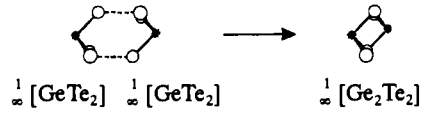

Scheme X

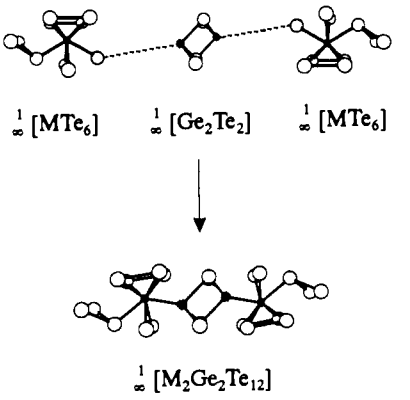

Scheme XI

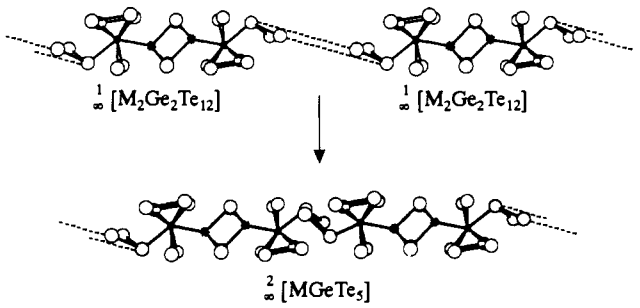

of the striking resemblance of $TiGeTe_6$ to $ZrTe_5$ and $HfTe_5$, it is surprising that "$TiTe_5$" has not been made, despite numerous attempts.[81]

There is now an alternative description of the $TiGeTe_6$ chain. The double Ge chain $^1_\infty[Ge_2Te_2]$ is nothing but a fragment of the layered structure of GeTe (isostructural with As) (Scheme IX).[85-87,97] Thus, the chain in $TiGeTe_6$ can also be viewed as resulting from the insertion of the $^1_\infty[Ge_2Te_2]$ chain between bicapped trigonal prismatic $^1_\infty[MTe_6]$ chains (Scheme X).

Instead of simply loosely associating the $^1_\infty[M_2Ge_2Te_{12}]$ chains to form the structure of $TiGeTe_6$, we speculate that it should be possible to condense them (through the two-atom arms, in the same fashion as in Scheme VII) to form a true two-dimensional layer $^2_\infty[MGeTe_5]$ (Scheme XI). This hypothetical phase, $MGeTe_5$, has a composition that is very close to those of the known phases $HfGeTe_4$ and $TiGeTe_6$, and precise conditions would likely be required for its synthesis.

3. Electrical Conductivity and Magnetic Susceptibility. Table VI provides a summary of the electrical and magnetic data. Plots of the relative electrical conductivity along the needle axis *a* of $ZrGeTe_4$ and $HfGeTe_4$ are given in Figure 7. The curves are similar to those adopted by doped semiconductors,[98,99] with a saturation region of nearly constant conductivity at intermediate temperatures (~160–180 K for $ZrGeTe_4$; ~150–200 K for $HfGeTe_4$), where the carrier concentration is constant. However, the slight temperature dependence of the carrier mobility imparts

Table VI. Electrical and Magnetic Data for $ZrGeTe_4$, $HfGeTe_4$, and $TiGeTe_6$

compound	$ZrGeTe_4$	$HfGeTe_4$	$TiGeTe_6$
σ_{300}, Ω^{-1} cm^{-1} [a]	~45	~10	~20
$\chi_{m,300}$, emu mol^{-1} [b]	-1×10^{-4} (?)	$-2.2(5) \times 10^{-4}$	$-1.1(6) \times 10^{-4}$
E_g, eV[c]	0.11(3)	0.18(2)	0.20(3)
remarks	semiconductor	semiconductor	transition from metal to semiconductor below ~165 K

[a] Average values measured along the needle axis of single crystals. [b] Uncorrected for core diamagnetism. As the $ZrGeTe_4$ sample is contaminated with diamagnetic impurities, the value shown is reliable to only an order of magnitude. [c] Calculated from the high-temperature data of $ZrGeTe_4$ and $HfGeTe_4$ and the low-temperature data of $TiGeTe_6$.

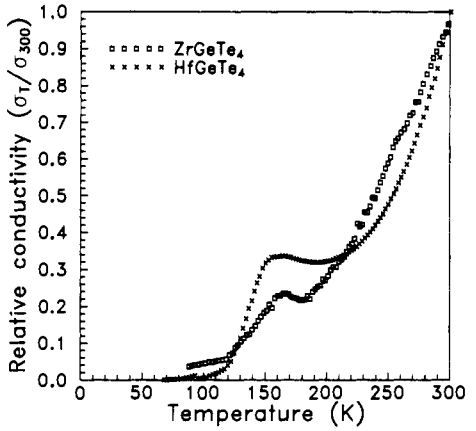

Figure 7. Plots of relative electrical conductivity along the needle axis *a* for single crystals of $ZrGeTe_4$ and $HfGeTe_4$. At room temperature, the conductivities are 44.2 and 3.0 Ω^{-1} cm^{-1} for $ZrGeTe_4$ and $HfGeTe_4$, respectively.

a small slope to the curve in this region. We suggest two possible sources for the extrinsic conductivity behavior. The Zr and Hf starting materials have nominal purities of 99.9% and 99.6%, respectively. The generally lower absolute conductivities (σ_{300} = ~10 Ω^{-1} cm^{-1}) and the wider saturation region in $HfGeTe_4$ are consistent with the lower purity of the Hf used. There is also evidence of Hf deficiencies from the crystal structure determination of $HfGeTe_4$. Vacancies in a crystal can produce acceptor levels that mimic the effects of impurity doping.[100] Measurements on a number of samples show wide variability, suggesting that the levels of impurities or nonstoichiometry are not constant among different crystals. From least-squares fits of the high-temperature data for several crystals, band gaps of 0.11(3) and 0.18(2) eV were calculated for $ZrGeTe_4$ and $HfGeTe_4$, respectively.

A plot of the relative electrical conductivity along the needle axis *b* of $TiGeTe_6$ is shown in Figure 8. The compound $TiGeTe_6$ appears to undergo a transition from metallic to semiconducting behavior when the temperature is decreased below ~165 K. Because of the difficulty in obtaining accurate crystal dimensions, the absolute values of the conductivity (σ_{300} = ~20 Ω^{-1} cm^{-1}) vary in measurements on different crystals, but the relative values show good consistency. On the assumption that the conductivity below the transition temperature can be described by the term $\exp(-E_a/kT)$ (or $\exp(-E_g/2kT)$), the activation energy calculated from a least-squares fit of the low-temperature data is E_a = 0.10(2) eV (or E_g = 0.20(3) eV). We present possible origins for this apparent metal-to-semiconductor transition later.

The compounds $TiGeTe_6$, $ZrGeTe_4$, and $HfGeTe_4$ display essentially temperature-independent magnetic susceptibilities of

(97) Hulliger, F. In *Structural Chemistry of Layer-Type Phases*; Lévy, F., Ed.; Physics and Chemistry of Materials with Layered Structures 5; D. Reidel: Dordrecht, Holland, 1976; pp 234–242.
(98) Cox, P. A. *The Electronic Structure and Chemistry of Solids*; Oxford University Press: Oxford, England, 1987.
(99) Ashcroft, N. W.; Mermin, N. D. *Solid State Physics*; Saunders College: Philadelphia, PA, 1976.
(100) Morgan, D. V.; Board, K. *An Introduction to Semiconductor Microtechnology*, 2nd ed.; Wiley: New York, 1990.

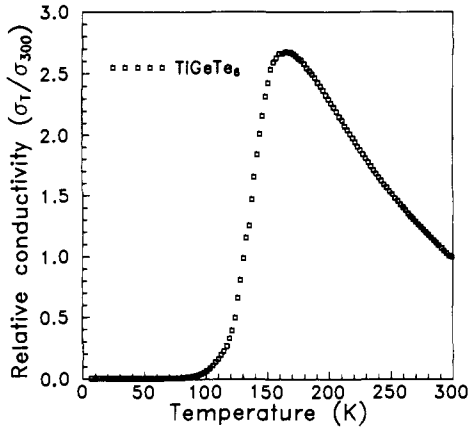

Figure 8. Plot of relative electrical conductivity along the needle axis *b* for a single crystal of $TiGeTe_6$. At room temperature, the conductivity is 21.8 Ω^{-1} cm $^{-1}$.

$-1.1(6) \times 10^{-4}$, -1×10^{-4}, and $-2.2(5) \times 10^{-4}$ emu mol^{-1}, respectively. When these values are corrected for core diamagnetism they become $+3.2(6) \times 10^{-4}$, $+2 \times 10^{-4}$, and $+0.8(5) \times 10^{-4}$ emu mol^{-1}, respectively, although this correction is rather uncertain. When the uncertainties in the corrected values are taken into account, the susceptibility of $TiGeTe_6$ is positive, while that of $HfGeTe_4$ could be positive or negative. Unfortunately we have been unable to obtain a sufficiently pure sample of $ZrGeTe_4$, and so the value of its susceptibility is reliable only within an order of magnitude. All samples show a small increase in susceptibility below ~50 K, which we attribute to trace amounts of paramagnetic impurities. There are no abrupt changes in the magnetic susceptibility near the electrical transition temperature in $TiGeTe_6$.

4. Electronic Structure. In order to rationalize some of the structural features and physical properties of $ZrGeTe_4$ and $TiGeTe_6$, we now examine their electronic band structures. The general conclusions reached for $ZrGeTe_4$ are readily extended to the isostructural $HfGeTe_4$.

a. Molecular Orbital Calculations. From the energy levels of the *molecular* building blocks that make up the extended structures of $ZrGeTe_4$ and $TiGeTe_6$, we can understand the origin of the bands in the band structures. Figure 9 shows the energy levels of some smaller molecular units. In $ZrGeTe_4$, the $[ZrGeTe_{10}]^{10-}$ bicapped trigonal prismatic cluster (b) is the important building block. As suggested earlier from the structural data (vide supra), we initially assume oxidation states Ge(II) and Te(−II) (as found in GeTe)[97] and Zr(IV) and Te(−II), with Te(−I) being assumed for the atoms in the Te–Te bond (as found in $ZrTe_3$).[73] The $[ZrGeTe_{10}]^{10-}$ cluster can be decomposed into two fragments, a $[GeTe_3]^{4-}$ trigonal pyramid (c) serving as a capping ligand at the open site of a $[ZrTe_7]^{6-}$ monocapped trigonal prism (a). In this $[ZrTe_7]^{6-}$ fragment, the unoccupied Zr d_{yz} orbital has a lobe that points out to the empty capping site and can thus potentially serve as a suitable acceptor orbital. If the cap were simply a Te^{2-} anion, with 5p orbitals at −13.2 eV, Zr–Te bonding levels would be formed that were largely of Te character, located at the lower end of the Te 5p block. However, the $[GeTe_3]^{4-}$ ligand (c) has a donor orbital, occupied by a lone pair, that is closer in energy (−10.7 eV) to that of the metal acceptor orbital (−9.1 eV). The Zr–Ge σ-bonding orbital thus formed in $[ZrGeTe_{10}]^{10-}$ (b) has large contributions of *both* Zr and Ge orbital character. When this Zr–Ge σ orbital is filled in $[ZrGeTe_{10}]^{10-}$, partial charge transfer should occur from Ge(II) to Zr(IV) (the initially assumed oxidation states). The reduction of Zr(IV) is consistent with the difference in the gross atomic populations in Te-capped $[ZrTe_8]^{8-}$ vs Ge-capped $[ZrGeTe_{10}]^{10-}$. While the gross atomic populations on respective Te atoms do not differ much, there are 0.5 more electrons in Zr in $[ZrGeTe_{10}]^{10-}$ than in $[ZrTe_8]^{8-}$. Since it is well established that Zr exists in the IV oxidation state in $ZrTe_3$ (in which $[ZrTe_8]^{8-}$ appears),[73] it should be more reduced in $ZrGeTe_4$ (in which $[ZrGeTe_{10}]^{10-}$ appears).

A similar analysis can be made for the $[TiGeTe_{12}]^{10-}$ cluster (d) that appears in $TiGeTe_6$. Again the cluster may be envisioned as being composed of a $[TiTe_9]^{6-}$ monocapped trigonal prismatic fragment (e) ligated by a $[GeTe_3]^{4-}$ trigonal pyramidal fragment (c). The additional Te–Te interactions (Te(1)–Te(6), 3.146(5) Å, and Te(3)–Te(4), 3.177(6) Å, shown in Figure 6b as dotted lines) create Te–Te antibonding levels that raise the top edge of the Te 5p block in $[TiTe_9]^{6-}$ (e) relative to that in $[ZrTe_7]^{6-}$ (a). The suitable acceptor orbital in $[TiTe_9]^{6-}$ is a mixture of Ti d_{z^2} and d_{xz} character. Because the d levels of Ti are lower in energy than those of Zr, the energy matching between the Ti acceptor and Ge donor orbitals is better, resulting in a greater stabilization of the Ti–Ge σ-bonding orbital.[101] We expect a reduction of Ti(IV) in this situation as well. Note that the presence of the largely $d_{x^2-y^2}$ orbital, whose lobes point away from the Te atoms, should give rise to a very localized band in the extended solid. The $d_{x^2-y^2}$ orbital and the top of the Te 5p block are separated by only 0.5 eV, and they will likely overlap in the solid.

b. $ZrGeTe_4$. The energy levels of the metal clusters now broaden into bands in the extended solid. As shown in Figure 10a, the density of states (DOS) curve for $ZrGeTe_4$ retains the general features of the molecular energy levels for $[ZrGeTe_{10}]^{10-}$ (Figure 9b). From the atomic projections of each element, we see that the DOS curve separates into clearly defined regions: below −10 eV is the wide anionic Te band; above −10 eV are the narrow cationic Zr bands that correspond to the original d levels in Figure 9b.

Semiconducting behavior is predicted, for the Fermi level lies in a gap between the Te valence band and the Zr $d_{x^2-y^2}$ conduction band. The band dispersion along the a^*, b^*, and c^* directions is shown in Figure 11. While the conduction band minimum is strictly at the point marked c in Figure 11, it is only slightly lower in energy than at point b, so that direct transitions from a to b occur at energies very close to the indirect band-gap energy from a to c. The energy gap at Γ is fairly small, E_g = 0.6 eV. Reasonable variations in the Te 5p H_{ii} parameter (−12.8 to −14.0 eV) resulted in band gaps ranging from 0.6 to 0.8 eV, which are relatively low values for a semiconductor.[102] Some caution[103] should be exercised in interpreting these results and relating them to the observed band gaps ($ZrGeTe_4$, 0.11(3) eV; $HfGeTe_4$, 0.18(2) eV). The band-structure calculations have been done for the hypothetically stoichiometric compound $ZrGeTe_4$, while the actual compound is expected to be nonstoichiometric, as suggested by the crystal structure determination of $HfGeTe_4$. If a rigid band scheme is assumed, a Zr-deficient compound would be metallic, since fewer electrons would move the Fermi level into the valence band. However, such a rigid band model is likely to be inadequate. Rather, one might expect Anderson localization,[98] owing to the randomness introduced by the Zr vacancies and the relaxation of the Te positions around these vacancies. If this were the case, the gaps inferred from the electrical measurements would have little to do with the band gap calculated for a stoichiometric compound. Rather, the gap would be related to the amplitude of the random potential. Further, one would expect to find a power-law behavior for the conductivity at a sufficiently low temperature. But the conductivity would need to be measured over many orders of magnitude to differentiate this behavior from an exponential decrease.

The bands are relatively disperse along the ΓX and ΓZ directions, which lie within the plane of the layers in $ZrGeTe_4$.

(101) Albright, T. A.; Burdett, J. K.; Whangbo, M.-H. *Orbital Interactions in Chemistry*; Wiley: New York, 1985.
(102) Kittel, C. *Introduction to Solid State Physics*, 6th ed.; Wiley: New York, 1986.
(103) We are indebted to an anonymous reviewer for insightful remarks concerning the electronic structures.

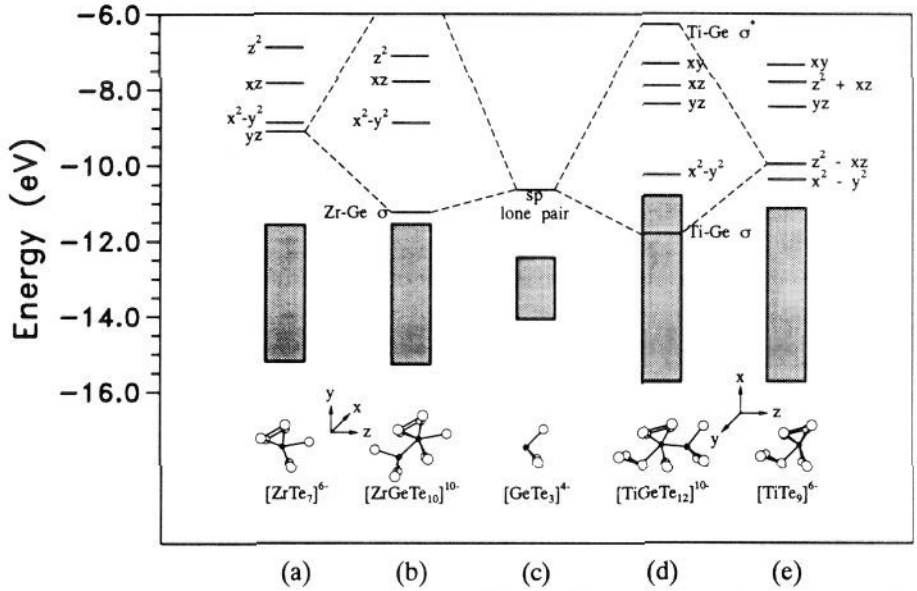

Figure 9. Molecular orbital energies of various fragments in $ZrGeTe_4$ and $TiGeTe_6$. The shaded rectangles represent a wide manifold of primarily Te 5p levels. The major contributions to the metal d levels are indicated. Combination of the (a) $[ZrTe_7]^{6-}$ and (c) $[GeTe_3]^{4-}$ fragments produces the (b) $[ZrGeTe_{10}]^{10-}$ cluster found in $ZrGeTe_4$. Combination of the (e) $[TiTe_9]^{6-}$ and (c) $[GeTe_3]^{4-}$ fragments produces the (d) $[TiGeTe_{12}]^{10-}$ cluster found in $TiGeTe_6$.

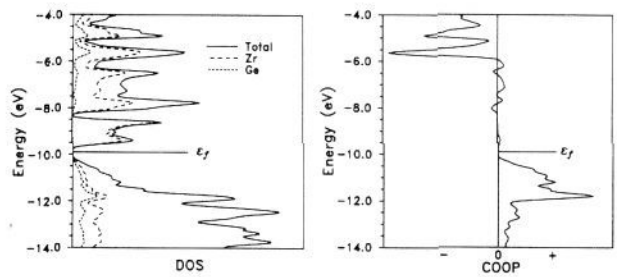

Figure 10. (a) Density of states (DOS) curve for $ZrGeTe_4$. The Zr and Ge contributions are represented by long and short dashed lines, respectively. The Fermi level lies in the gap near −10 eV. (b) Crystal orbital overlap population (COOP) curve for the Zr–Ge contacts in $ZrGeTe_4$. Positive and negative values of COOP correspond to bonding and antibonding character, respectively.

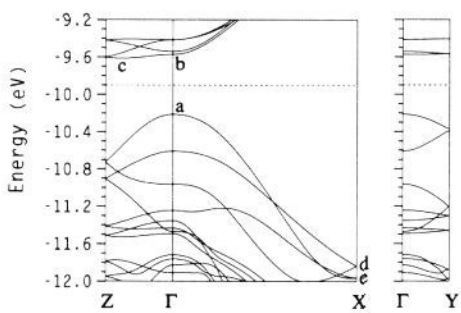

Figure 11. Calculated electronic band dispersion in $ZrGeTe_4$ along a^*, b^*, and c^*. $\Gamma = (0, 0, 0)$, $X = (^1/_2, 0, 0)$, $Y = (0, ^1/_2, 0)$, and $Z = (0, 0, ^1/_2)$. The Fermi level is represented by the dashed line. The letters denote convenient reference points for the discussion in the text.

Other directions in the Brillouin zone that are parallel to this plane show similar breadth in their bands, consistent with strong *intralayer* bonding. However, along the direction ΓY, perpendicular to the layers and parallel to the stacking axis, the bands are narrower, consistent with weak *interlayer* interactions. Because interlayer interactions are sometimes important in the integrity of layered tellurides,[76,104] we calculated the integrated overlap populations (IOPOP) for all Te–Te contacts less than 4.0 Å. The shortest interlayer Te–Te contact (3.604(2) Å) has a negative IOPOP (−0.006 e/bond). In fact, all the Te–Te contacts have slightly negative IOPOPs, with the exception of the short Te(3)–Te(4) contact (2.737(2) Å), whose large positive value (+0.524 e/bond) definitely classifies it as a Te–Te single bond. Since there is no evidence of interlayer Te–Te interactions, $ZrGeTe_4$ and $HfGeTe_4$ may be viewed as true two-dimensional structures whose layers are held together primarily by weak van der Waals forces. Variations in the k-point mesh size used in calculating the IOPOPs do not alter these conclusions.

The Zr–Ge bonding is of particular interest. From the composition of the crystal orbitals, the Zr–Ge bonding levels are found to cluster mainly between −11 and −12 eV. For example, the crystal orbitals near −11.8 eV (d and e in Figure 11) have large contributions of Zr d_{yz} and Ge sp orbital character in the same orientation as found in the molecular orbitals (Figure 9b) to produce strong Zr–Ge σ bonding. The large positive (at −11.8 eV) and negative (at −5.6 eV) peaks in the crystal orbital overlap population (COOP) curve for Zr–Ge contacts (Figure 10b) correspond to the Zr–Ge bonding and antibonding levels, respectively, near the energies found in the molecular clusters (Figure 9b). At the Fermi level, most of the Zr–Ge bonding levels are filled, consistent with strong Zr–Ge bonding. From the molecular point of view, the Zr–Ge bond is nothing more than a donor–acceptor interaction, accompanied by a reduction of Zr(IV) to Zr(III) and oxidation of Ge(II) to Ge(III). Because the lone d electron in Zr(III) (d^1) is involved in the Zr–Ge bond, there are no unpaired spins, and the compound $ZrGeTe_4$ (as well as $HfGeTe_4$) should be diamagnetic.[105] Ge(III) is not an unprecedented oxidation state, appearing in the compounds $LiGeTe_2$,[106] $Na_6Ge_2Te_6$,[88] $Na_8Ge_4Te_{10}$,[107,108] $K_6Ge_2Te_6$,[89] Tl_6-

(104) Jobic, S.; Brec, R.; Rouxel, J. *J. Solid State Chem.* **1992**, *96*, 169–180.

(105) Experimentally, the measured magnetic susceptibilities of $ZrGeTe_4$ and $HfGeTe_4$ are negative, but the signs of the corrected susceptibilities are in doubt, owing to the large uncertainties in these values.

(106) Eisenmann, B.; Schwerer, H.; Schäfer, H. *Mater. Res. Bull.* **1983**, *18*, 1189–1194.

(107) Eisenmann, B.; Schwerer, H.; Schäfer, H. *Rev. Chim. Miner.* **1983**, *20*, 78–87.

(108) Eisenmann, B.; Schäfer, H.; Schwerer, H. *Z. Naturforsch., B: Anorg. Chem., Org. Chem.* **1983**, *38*, 924–929.

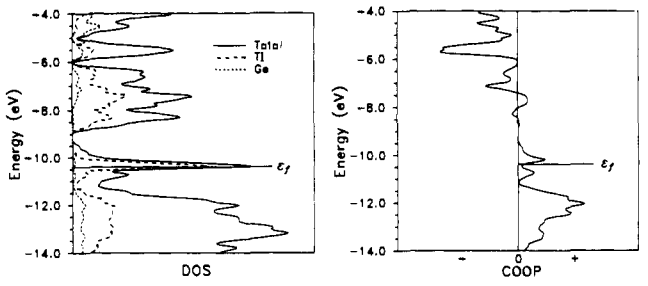

(a) (b)

Figure 12. (a) Density of states (DOS) curve for $TiGeTe_6$. The Ti and Ge contributions are represented by long and short dashed lines, respectively. The Fermi level is at −10.4 eV. (b) Crystal orbital overlap population (COOP) curve for the Ti–Ge contacts in $TiGeTe_6$.

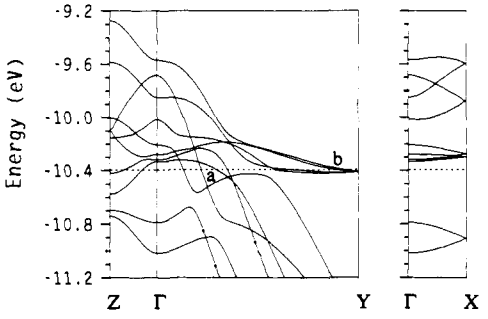

Figure 13. Calculated electronic band dispersion in $TiGeTe_6$ along a^*, b^*, and c^*. $\Gamma = (0, 0, 0)$, $X = (^1/_2, 0, 0)$, $Y = (0, ^1/_2, 0)$, and $Z = (0, 0, ^1/_2)$. The Fermi level is represented by the dashed line. The letters denote convenient reference points for the discussion in the text.

Ge_2Te_6,[109] and $Ba_2Ge_2Te_5$,[90] all of which contain Ge bonded to itself as well as to three Te atoms. Thus a plausible valence description is $Zr^{3+}Ge^{3+}(Te_2^{2-})(Te^{2-})_2$ for the stoichiometric compound $ZrGeTe_4$. If the nonstoichiometry observed in the crystal structure determination of $HfGeTe_4$ is general, then necessarily the cationic deficiencies must lead to mixed valency, e.g., Zr^{3+} and Zr^{4+}.

c. $TiGeTe_6$. The DOS curve for $TiGeTe_6$ is given in Figure 12a. Again, the features present in the molecular energy diagram (Figure 9d) are preserved in the bands of the solid. Above −9.0 eV are the narrow cationic Ti d bands. Below −9.0 eV, the narrow Ti $d_{x^2-y^2}$ band now overlaps with the anionic Te band.

Metallic behavior for $TiGeTe_6$ is predicted, for the Fermi level crosses partially filled bands, as shown in the band dispersion diagram in Figure 13. The most disperse bands crossed by the Fermi level, near **a**, are along the ΓY direction, corresponding to the b^* axis, consistent with the metallic conductivity observed along the needle axis. Less disperse bands are also crossed along the ΓZ direction (c^*), approximately along the layer perpendicular to the one-dimensional chains, while no bands are crossed along the ΓX direction (a^*), perpendicular to the layers. (Only when the Te 5p H_{ii} parameter is set to the low value of −13.60 eV does the Fermi level touch the bottom of the narrow band along ΓX.) Inspection of bands in other symmetry directions in the Brillouin zone suggests that electrical conductivity should be most facile along the direction of the one-dimensional chains, possible along the layers perpendicular to these chains, and not likely at all between the layers. Examination of the orbital composition of the wide band along ΓY suggests that conduction is probably mediated through the Te and Ti atoms, via $Te_{p\pi}$–$Ti_{d\pi}$ interactions along the chain direction.

Conductivity measurements indicate that while $TiGeTe_6$ is metallic above ~165 K, it is semiconducting at lower temperatures. The metal-to-semiconductor transition is not a first-order one, as neither abrupt changes in the cell parameters between 100 and 200 K nor any obvious transition in magnetic susceptibility near 165 K is observed. The DOS curve (Figure 12a) shows that the Fermi level crosses very narrow bands near −10 eV. These bands (**b** in Figure 13) are almost exclusively of Ti $d_{x^2-y^2}$ nonbonding character. Electrons can become localized in these narrow bands as a result of electron repulsion effects, which are not treated explicitly in the present one-electron model. It is possible that $TiGeTe_6$ becomes a Mott–Hubbard semiconductor[98,99] below the transition temperature, with an activation energy proportional to the electron repulsion energy.

An alternative interpretation[103] is that the conductivity of $TiGeTe_6$ between 165 and 300 K (Figure 8) does not arise from "metallic" conduction. Rather, the mobility of carriers from impurities may be increasing with decreasing temperature while the carrier concentration is nearly constant, resulting in a plot similar to that for $ZrGeTe_6$ (Figure 7), only more pronounced and shifted in temperature. If so, the conductivity above 300 K should go through a minimum and then increase. Moreover, the conductivity of $TiGeTe_6$ at 300 K is relatively low (~20 Ω^{-1} cm^{-1}) compared to those of typical metallic compounds (>10^3 Ω^{-1} cm^{-1}). Thus, $TiGeTe_6$ could be a semiconductor because of the occurrence of charge density waves, a feature that would have to be detected by more sensitive techniques, such as electron diffraction.

There is a wide range of Te–Te distances in $TiGeTe_6$. Of all the Te–Te contacts in the structure that are less than 4.0 Å, only five have positive IOPOPs. The strongest bonds are Te(4)–Te(5) (2.812(6) Å) and Te(3)–Te(6) (2.901(4) Å) with large IOPOPs of 0.421 and 0.409 e/bond, respectively. These distances, which are comparable to those of the corresponding bonds in $HfTe_5$ (2.763(4) and 2.908(3) Å, respectively), we consider to be full Te–Te single bonds. But some secondary bonds, namely Te(1)–Te(6) (3.146(5) Å) and Te(3)–Te(4) (3.177(6) Å), have IOPOPs of 0.144 and 0.114 e/bond, respectively, about a quarter of those of the full single bonds. Finally, there is the intriguing Te(3)–Te(3) contact (3.492(6) Å), whose small but nonnegligible IOPOP of 0.024 e/bond implies some degree of tertiary bonding. As the Te(3)–Te(3) contact is the *only* link between the one-dimensional $^1_\infty[Ti_2Ge_2Te_{12}]$ chains, we may describe the $TiGeTe_6$ structure as consisting of noninteracting layers (only van der Waals forces) that in turn comprise weakly bonded one-dimensional chains. These results are unchanged when the k-point mesh size is varied.

Alternatively, the strengths of these Te–Te bonds can be compared through the use of the valence bond method.[110] The bond valences of the short Te–Te contacts ($d < 4.0$ Å) in $HfGeTe_4$ and $TiGeTe_6$ were calculated from the formula $\nu = \exp[(R - d)/0.37]$, based on the bond valence parameter R of 2.76 Å for a Te–Te single bond.[111] As shown in Figure 14, the IOPOPs and bond valences for these Te–Te contacts are well-correlated. The general trend holds that lower IOPOPs and lower bond valences correspond to weaker bonding. Because the IOPOP values also depend on the directionality of orbital overlap, the 2.901(4)-Å Te–Te contact in $TiGeTe_6$ is stronger than would be expected on the basis of bond distances alone.

The Ti–Ge bonding in $TiGeTe_6$ arises from the same type of donor–acceptor interaction as found in $ZrGeTe_4$. In the COOP curve for the Ti–Ge contacts, shown in Figure 12b, the bonding (at −12.0 eV) and antibonding (at −5.5 eV) levels are evident, near the energies originally found in the molecular cluster (Figure 9d). If we accept the oxidation states Ti(III) and Ge(III), in analogy to $ZrGeTe_4$, then the average oxidation state of Te in $TiGeTe_6$ is Te(−I). That Te is not fully reduced is a reflection

(109) Eulenberger, G. *J. Solid State Chem.* **1984**, *55*, 306–313.

(110) Brown, I. D. In *Structure and Bonding in Crystals*; O'Keeffe, M., Navrotsky, A., Eds.; Academic Press: New York, 1981; Vol. II, Chapter 14, pp 1–30.

(111) Brese, N. E.; O'Keeffe, M. *Acta Crystallogr., Sect. B: Struct. Sci.* **1991**, *47*, 192–197.

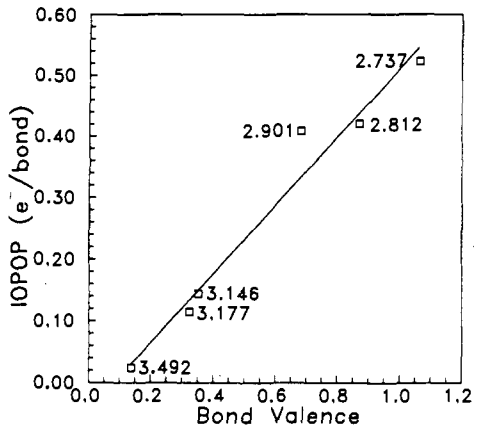

Figure 14. Plot of IOPOP vs bond valence for short Te–Te distances (Å) in $HfGeTe_4$ and $TiGeTe_6$. The 2.737(2)-Å distance appears in $HfGeTe_4$, while the other distances appear in $TiGeTe_6$.

of the much more extensive Te–Te bonding present in this structure. The inclusion of secondary Te–Te bonding (Te(1)–Te(6) and Te(3)–Te(4)) precludes a straightforward assignment of formal oxidation states to individual Te atoms because the Te(4)–Te(5) and Te(3)–Te(6) single bonds cannot be considered independently of the subsidiary Te–Te interactions.

Conclusion

The interesting new compounds $TiGeTe_6$, $ZrGeTe_4$, and $HfGeTe_4$ have been synthesized, and their structural and physical properties have been investigated both experimentally and through band-structure calculations. The phases $MGeTe_4$ (M = Zr, Hf) and $TiGeTe_6$ are structurally analogous to the binary phases $ZrTe_3$ and $HfTe_5$, respectively. Both have two-dimensional structures whose layers are held together only by van der Waals forces, but in $TiGeTe_6$, the layers comprise one-dimensional chains that are held together weakly by a long Te–Te bond. A novel feature in these compounds is the metal–Ge bond, viewed as arising from a donor–acceptor interaction between the lone pair of a $[GeTe_3]^{4-}$ trigonal pyramid and a vacant d orbital on the metal. While the $MGeTe_4$ (M = Zr, Hf) compounds are semiconductors, they are also probably deficient in M. $TiGeTe_6$ is semiconducting below ~165 K and apparently metallic above. The cause of this transition is unclear.

The association of polyhedral building blocks allows us to postulate the existence of new hypothetical phases, such as $MGeTe_5$. It may be interesting to try substituting Ge with Si, whose orbital energies are lower but whose orbital extents are smaller.[17] Attempts in both these directions are currently underway.

Acknowledgment. This work was supported by the U.S. National Science Foundation through Grant DMR-91-14934. Use was made of the SEM, electrical conductivity, and magnetic susceptibility facilities of the Materials Research Center at Northwestern University (U.S. National Science Foundation Grant DMR-91-20521). We thank Dr. Stéphane Jobic for helpful discussions of the band-structure calculations.

Supplementary Material Available: Crystallographic and refinement details (Table IS) and anisotropic thermal parameters (Table IIS) (3 pages); observed and calculated structure amplitudes (×10) (Table IIIS) (12 pages). Ordering information is given on any current masthead page.